Methylglyoxal Produced by Amyloid β-Peptide-Induced Nitrotyrosination of Triosephosphate Isomerase Triggers Neuronal Death in Alzheimer Disease

Marta Tajes[a], Abel Eraso-Pichot[a], Fanny Rubio-Moscardó[a], Biuse Guivernau[a], Eva Ramos-Fernández[a], Mònica Bosch-Morató[a], Francesc Xavier Guix[a], Jordi Clarimón[b], Gian Pietro Miscione[c,d], Mercé Boada[e,f], Gabriel Gil-Gómez[g], Toshiharu Suzuki[h], Henrik Molina[i], Jordi Villà-Freixa[c,j], Rubén Vicente[a] and Francisco J. Muñoz[a *]

[a]Laboratory of Molecular Physiology and Channelopathies, Departament de Ciències Experimentals i de la Salut (DCEXS), Universitat Pompeu Fabra (UPF), Barcelona, Spain

[b]Alzheimer Laboratory, Neurology Department, Hospital de la Santa Creu i Sant Pau, Barcelona, Centro de Investigación Biomédica en Red sobre Enfermedades Neurodegenerativas (CIBERNED)

[c]Computational Biochemistry and Biophysics Laboratory, Research Program on Biomedical Informatics, DCEXS, IMIM/UPF, Barcelona

[d]Dipartimento di Chimica "G. Ciamician", Università degli Studi di Bologna, Italy

[e]Memory Clinic, Fundació ACE. Institut Català de Neurociències Aplicades, Barcelona

[f]Neurology Department, Hospital Universitari Vall d'Hebron- Institut de Recerca, Universitat Autònoma de Barcelona (VHIR-UAB), Barcelona

[g]IMIM (Institut Hospital del Mar d'Investigacions Mèdiques). Barcelona

[h]Laboratory of Neuroscience, Graduate School of Pharmaceutical Sciences, Hokkaido University, Sapporo, Japan

[i] Proteomics Unit, DCEXS, UPF and Centre de Regulació Genòmica (CRG); Barcelona

[j]Escola Politècnica Superior, Universitat de Vic, Spain

Running title: Methylglyoxal in Aß-induced apoptosis

* To whom correspondence should be addressed: Dr. Francisco J. Muñoz, Lab. Fisiologia Molecular i Canalopaties, Departament de Ciències Experimentals i de la Salut, Universitat Pompeu Fabra, C/ Dr. Aiguader 88, Barcelona 08003, Spain; Tel: +34 93 316 08 52; Fax: +34 93 316 09 01; e-mail: paco.munoz@upf.edu

Abstract

Amyloid-β peptide (Aβ) aggregates induce nitro-oxidative stress, contributing to the characteristic neurodegeneration found in Alzheimer disease (AD). One of the most strongly nitrotyrosinated proteins in AD, the triosephosphate isomerase (TPI) enzyme, regulates glycolytic flow, which decreases its efficiency. The main aims of this study were to analyze the impact of TPI nitrotyrosination on cell viability and to identify the mechanism behind this effect. In human neuroblastoma cells (SH-SY5Y), we evaluated the effects of $A\beta_{42}$ oligomers on TPI nitrotyrosination. We found an increased production of methylglyoxal (MG), a toxic by-product of the inefficient nitro-TPI function. The proapoptotic effects of $A\beta_{42}$ oligomers, such as decreasing the protective Bcl2 and increasing the proapoptotic caspase-3 and Bax were prevented with a methylglyoxal chelator. Moreover, we used a double mutant TPI (Y165F and Y209F) to mimic nitrosative modifications due to Aβ action. Neuroblastoma cells transfected with the double mutant TPI consistently triggered MG production and a decrease in cell viability due to apoptotic mechanisms. Our data show for the first time that MG is playing a key role in the neuronal death induced by Aβ oligomers. This occurs because of TPI nitrotyrosination, which affects both tyrosines associated with the catalytic center.

Keywords: Alzheimer disease; 3- nitrotyrosine; amyloid; triose-phosphate isomerase; apoptosis; methylglyoxal

Abbreviations: Ab, Antibody; Aß, Amyloid-ß peptide; AD, Alzheimer disease; AG, aminoguanidine; AGEs, advanced glycation end-products; DHAP, dihydroxyacetone phosphate; FBS, fetal bovine serum; GAP, D-glyceraldehyde 3-phosphate; H_2O_2, hydrogen peroxide; MG, methylglyoxal; MTT, 3-(4,5-dimethylthiazol-2-yl)-2,5-diphenyltetrazolium bromide; NO, nitric oxide; nNOS, neuronal NO synthase; SIN-1, 3-morpholino-sydnonimine; o.e., overexpressing; TPI, triosephosphate isomerase; YY TPI, mutant Tyr165Phe and Tyr209Phe TPI; WT, Wild type**.**

Introduction

Amyloid-β peptide (Aβ) aggregates produce free radicals [1-3] that damage membrane proteins such as ATPases and ion channels, leading to an increase in intracellular calcium levels [4,5]. Under these conditions, nitric oxide (NO) is produced by the activation of the neuronal NO synthase (nNOS), a Ca^{2+}-calmodulin-dependent enzyme [6,7]. NO can react with other molecules such as superoxide anion ($O_2^{\cdot-}$) to form peroxynitrite anion ($ONOO^{\cdot-}$) [8], a short-lived but highly reactive molecule that nitrotyrosinates proteins. This modification is an irreversible reaction that adds a nitro group (NO_2) to a tyrosine residue, generating 3-nitrotyrosine [9,10]. Consequently, nitrotyrosination is widespread in Alzheimer disease (AD) brain [11,12]; antioxidants such as free radical scavengers [13] or inhibitors of NO production have been proposed to protect against Aβ toxicity [14].

One of the proteins strongly nitrotyrosinated by Aβ action is triosephosphate isomerase (TPI) [15,16]. TPI catalyzes the interconversion of D-glyceraldehyde-3-phosphate (GAP) to dihydroxyacetone phosphate (DHAP). A key enzyme in cell metabolism, TPI controls glycolytic flow and ensures efficient energy production [17], which is essential to support normal cell activity.

Glucose is the primary source of energy for the brain. Any interruption of glycolysis causes brain dysfunction and memory loss, favoring neurodegeneration [18]. Isomerase deficiency is associated with neurodegeneration [19] and has been related to

reduced longevity [20]. Moreover, TPI deficiency leads to the accumulation of its substrate DHAP, which can decompose non-enzymatically into methylglyoxal (MG), a cytotoxic precursor of advanced glycation end-products (AGEs) [21]. MG acts as a potent glycative agent that triggers apoptosis in neurons [22,23]. Protein glycation has been previously reported in AD brains [16,24] and it would be contributing to the neuronal damage [25].

In AD patients, TPI is highly nitrotyrosinated [16,26,27]. We have previously reported that TPI nitrotyrosination by Aβ action reduces the efficiency of its isomerase activity and leads TPI to adopt a ß-sheet structure that favours Tau aggregation into paired helicoidal filaments (PHF), one of the AD hallmarks [16].

The present study analyzed the impact of nitro-TPI on cell viability, proposing MG production as the mechanism behind the deleterious consequences of Aβ-dependent TPI nitrotyrosination. We analyzed the toxic effects of treating neuroblastoma cells (SH-SY5Y) with $A\beta_{42}$ oligomers. In addition, we studied the effect of Tyr165 and Tyr209 nitration (located close to the catalytic center of the enzyme) using the Phe mutation of Tyr that mimics the nitro-TPI structure. A computationally validated model of nitro-TPI was used to analyze its effects.

Materials and Methods

Tissue samples

Human brain tissue sections were supplied by the Banc de Teixits Neurològics, Serveis Científico-Tècnics, Hospital Clínic, Universitat de Barcelona. Brain samples were obtained from the *gyrus frontalis superior* of the frontal cortex of five healthy individuals (3 males and 2 females aged 59.6±6.9 aged years) and five patients with AD, at stage VI (2 males and 3 females; aged 72±4.5 years). Human brain sample analysis was approved by

the Ethics Committee for Clinical Investigation of the Institut Municipal d'Investigacions Mèdiques, Universitat Pompeu Fabra (IMIM-UPF Approval ID: 2010/3847/I). Written informed consent was obtained for all study participants.

Immunohistochemistry of human brain samples

Frontal cortex sections (5 μm) were pre-treated with 50% formic acid for 1 min to expose TPI epitopes. Sections were incubated with rabbit anti-TPI polyclonal Ab (1:500, Abcam, Cambridge, UK) or anti-argpyrimidine Ab (1:500, Cosmo Bio Co., Ltd, Tokyo, Japan) for 2 h at room temperature (RT), then incubated with donkey anti-rabbit peroxidase-conjugated Ab (1:500) for 1 h at RT. Slides were treated with a DAB peroxidase substrate kit. Samples were counterstained with hematoxylin, dehydrated and fixed.

Mice brain samples

Cerebral paraffined slides from APPswe/PS1 L166P mice were deparaffined with Clear Rite 3 and washes with decreasing ethanol dilutions. Briefly, slides were blocked for 1 h at room temperature with 2% normal serum in TNB buffer. The same solution was used to dilute (1:100) the anti-argpyrimidine (Cosmobio) antibody. The primary antibody was incubated overnight at 4ºC. The secondary antibody was further diluted (1:200). All washes were performed with TNT 1X buffer. Mice dissection followed E.U. guidelines for animal experimentation and was approved by the Ethics Committee for Animal Experimentation (IMIM-UPF; Approval ID: JMC-07-1001P1-PML).

Overexpression of TPI in neuroblastoma cells

TPI was amplified by PCR from purified human chromosomal DNA and cloned into a construct containing a 5' upstream flag sequence. Wild-type (WT) TPI and TPI carrying double tyrosine mutation (Y165F/Y209F) were produced and subcloned into a pcDNA3 plasmid. A human neuroblastoma cell line (SH-SY5Y) was seeded in 6-well plates at a density of 5 x 10^5 cells per well and grown for 24 h with Dulbecco modified Eagle medium (DMEM) supplemented with 15% fetal bovine serum (FBS). Afterwards, 2 µg per well of each construct was transfected using Lipofectamine 2000 Reagent (Invitrogen, Carlsbad, USA), following manufacturer instructions. After 3 h, the medium was replaced by DMEM plus 15% FBS and 1% penicillin/streptomycin.

$A\beta_{42}$ oligomer preparation

Synthetic $A\beta_{42}$ (EZBiolab, Carmel, USA) oligomers were obtained by dissolving 300 µg freeze-dried aliquots in 20 µL DMSO. Peptide stock aliquots were diluted in 0.1 M Tris-HCl at pH 7.4 to a final concentration of 88.6 µM Aβ. Solutions were stirred continuously at 37ºC and 300 rpm for 3 h and kept at -80 ºC before being used (Fig. S1).

$A\beta_{42}$ oligomer incubation with human neuroblastoma cells

SH-SY5Y, a human neuroblastoma cell line (supplied by ECACC), was grown in DMEM (Invitrogen) supplemented with 15% FBS and 1% streptomycin/penicillin at 37ºC in a humidified atmosphere containing 5% CO2. For cell viability and metabolism assays, cells were seeded into 96-well culture plates at a density of 25,000 cells / 200 µL per well.

For Western blot analysis, cells were plated onto 60mm-diameter-dishes at a density of 700,000 cells / 3 mL per dish.

After 24 h in culture, cells were treated with different concentrations of Aβ oligomers (0.1, 0.5 and 1 μM) for another 24 h. Then the cells were lysed on ice with a solution containing 1 M Tris-HCl, 1% Nonidet P-40, 150 mM NaCl, 5 mM EDTA, 1 mM sodium orthovanadate, 1 mM dithiotreitol, pH 7.4, and a protease inhibitor cocktail. Protein concentration was determined by Bradford assay.

Treatment of SH-SY5Y with hydrogen peroxide (H_2O_2), camptothecin and scrambled Aβ

Cells were treated with different concentrations of scrambled WT $A\beta_{42}$ prepared as the WT $A\beta_{42}$ (0.1, 0.5 and 1 μM; rPeptide; Stratech Scientific), the pro-apoptotic inhibitor of DNA topoisomerase I camptothecin (10, 100, 500 and 1000 nM; Sigma) and H_2O_2, (1, 10, 100 and 200 μM; Sigma) for 24 h.

Treatment of SH-SY5Y with aminoguanidine (AG)

Cells were pre-treated with the MG scavenger AG (Sigma) at 250 μM for 1 h before the addition of Aβ oligomers for a 24 h treatment. In transfected cells, AG was added at the beginning of transfection.

Incubation of SH-SY5Y o.e. WT TPI with conditioned medium

Cells o.e. WT TPI were incubated during 24 h with the medium from cells o.e. WT or YY TPI (conditioned medium).

TPI immunoprecipitation

500 μg of total protein from brains or SH-SY5Y cells lysates were incubated with 1.25 μg of anti-TPI polyclonal antibody (Ab) o.n. at 4ºC. Protein G immobilized on sepharose was added and samples were shaken for 2 h at RT. Aggregates were pulled down by centrifugation at 10,000 rpm for 10 min and washed thrice. Protein G and Ab were removed from the immunoprecipitated proteins by boiling the samples for 6 min at 100 ºC.

Western blot

For analysis of cell homogenate aliquots, gels were transferred to PVDF membranes and incubated for 3 h at room temperature with one of 7 solutions: mouse anti-argpyrimidine monoclonal Ab (1:1,000; Cosmo Bio Co., Ltd), mouse anti-nitrotyrosine monoclonal Ab (1:1,000; Cayman Chemical, Michigan, USA), rabbit anti-cleaved caspase-3 (Asp175) Ab, rabbit anti-Bax Ab (1:1,000; Cell Signaling, Beverly, USA), mouse-anti TPI Ab (1:1000; Abcam), rabbit anti Bcl-2 Ab (1:1000; Cell Signaling), or mouse anti-β-actin monoclonal Ab (1:5,000, Sigma, St. Louis, USA). Membranes were incubated with peroxidase-conjugated secondary Ab (1:3,000; GE-Healthcare, UK) for 1 h at RT. Bands were visualized using the enhanced chemiluminescence substrate (Super Signal; Pierce).

Immunocytochemistry of SH-SY5Y

After 24h, cells were fixed with 4% paraformaldehyde and permeabilized with 0.1% Triton X-100. SH-SY5Y cells were immunostained with 1:100 mouse monoclonal anti-methylglyoxal Ab (Cosmo Bio Co., Ltd.) and 1:2,000 Alexa 555-bound as secondary Ab (Sigma) at RT. Transfected cells were positive for EGFP fluorescence. Coverslips were mounted and analyzed using a Leica TCS SP confocal microscope and analyzed with Leica confocal software.

Cell viability assays

SH-SY5Y cells were seeded in 96-well plates at a density of 25,000 cells / 200 μL, incubated 24 h, and tested for viability by 3-(4,5-dimethylthiazol-2-yl)-2,5-diphenyltetrazolium bromide (MTT) reduction. Briefly, 11 μL of MTT stock solution (5mg/mL) were added; after 2h the reaction was stopped with 120 μL of DMSO. MTT reduction was determined in a plate reader spectrophotometer at 540 and 650 nm. Control cells were taken as 100%.

Measurement of $\Delta\Psi_m$

SH-SY5Y cells were re-suspended at 10^6 cells/mL in PBS with the fluorophore MitoTracker Red CMXRos (Molecular Probes, Carlsbad, USA). Cells were incubated for 10 min at 37ºC and analyzed in a FACScan (Becton Dickinson, CA).

Liquid chromatography-Mass spectrometry (LC-MS/MS) experiments

Commercial TPI from rabbit (Sigma) was reduced and alkylated prior to trypsinization in solution. Tryptic peptides were desalted using C18 type stage tip41 [28] prior to analysis by reversed phase nano LC-MS/MS on an Orbitrap Velos (ThermoScientific, Bremen, Germany) mass spectrometer in higher-energy collisional dissociation (HCD) mode. MS/MS spectra were extracted using ProteomeDiscoverer 1.3 (ThermoScientific, Bremen Germany) and searched against SwissProt mammalian using MASCOT. Mass tolerance of 10 ppm and 20 mDa was used for precursor and fragment ions, respectively.

Computational modelling of the effect of Phe and nitroTyr substitutions on Y165 and Y209

Two structures were taken from the PDB as representatives of the open and closed states of TPI, namely 1I45 and 1NEY, respectively. The structures were processed with the Schrodinger's Maestro 9.2.109 suite for missing heavy atoms and hydrogens, as well as to transform fluoro-tryptophan residues into tryptophan. The optimal hydrogen bond network (providing optimal protonation states to His residues and optimizing the orientation of the protein side chains) was obtained with the protein preparation wizard in the same suite. Mutations were then introduced in order to build the Y165F and Y165*n* systems from the open-state wt structure (1I45) and the Y209F and Y209*n* systems from the closed-state wt structure (1NEY). The 6 structures were independently solvated with the Impact/soak module in maestro, in a cube of TIP3P water molecules with 60x60x60 $Å^3$ around the mass center of each protein. We ran 1ns molecular dynamics (MD) simulations with periodic boundary conditions and a 12 Å cut-off radius for non-bonded interactions (updating non-bonded lists every 10 steps) on the different systems, while keeping fixed the protein atoms

in order to relax the water molecule positions. After MD runs, the final snapshots were taken as input for the Quantum Mechanics/Molecular Mechanics (QM/MM) runs.

All QM/MM calculations were performed with the Qsite program, taking as QM region the residues directly involved in the hydrogen-bonding networks of interest. This involved residues 164-166 and the side chain of 169 in the open state and 176-178,208-210 in the closed state. With these settings, QM regions included 48 to 74 atoms, depending on the system. QM/MM minimizations where performed with a truncated Newton optimizer for the MM. A sphere of radius 10 Å was built around the centroid of the QM region to define the region to be minimized, leaving fixed throughout the simulation the water molecules beyond that radius. Density functional theory (DFT) computations using the non-local hybrid Becke three-parameter exchange function (denoted as B3LYP) with the 6-31G* basis set as implemented in Jaguar were chosen to describe the energy of the QM region and the frozen orbital method was used to describe the QM-MM interface. Molecular graphics images were produced using the UCSF Chimera package from the Resource for Biocomputing, Visualization, and Informatics at the University of California, San Francisco (supported by NIH P41 RR001081).

Genetic study of TPI polymorphisms

The biallelic polymorphism rs2001004, located in the first intron of the TPI, was selected to be typed because it has been validated and has an estimated minor allele frequency in European populations around 0.34 (www.hapmap.org). Genotyping was conducted by TaqMan Assays-on-Demand on the ABI PRISMs 7900HT Sequence Detection System (Applied Biosystems, Carlsbad, California), followed by analysis with SDS 7500 software, version 2.0.1 (Applied Byosystems, Carlsbad, California).

The SNP was typed in 231 individuals diagnosed with Alzheimer dementia (mean age at onset of 76.4±5.6 years, 73.5% women) and 136 cognitively healthy control individuals (mean age at blood extraction, 71.7±9.4 years; 58% women). For all patients, the diagnosis was established according to the National Institute on Neurological Disorders and Stroke, and the Alzheimer Disease and Related Disorders Association (NINDS-ADRDA) guidelines (Neurology 34(7):939-944). All samples were recruited from Fundació ACE and written informed consent was obtained from all participants or surrogates.

Statistical analysis

Data were expressed as the mean ± SEM of the values from the number of experiments as indicated in the corresponding figures. Continuous data were evaluated by Student *t*-test. Genotype and allele frequencies were estimated by direct counting and were compared between patients and controls by Chi-square analysis with one degree of freedom.

Results

TPI nitrotyrosination and the consequent MG production in AD are due to Aß action

As previously reported [16], we found that TPI is highly nitrotyrosinated in the brain of AD patients, as obtained by Western blot and nitrotyrosination quantification regarding the protein levels (Fig. 1A), where it forms big intracellular aggregates (Fig. 1B). Therefore, we prepared Aβ oligomers, characterized by Western blot analysis (Fig. S1),

and we found that the challenge of human neuroblastoma cells with increasing concentrations of Aβ oligomers produced a proportional increase in TPI nitrotyrosination (Fig. 1C), reinforcing that TPI nitrotyrosination is due to Aβ action [15,29].

MG is synthesized at a very low rate as a by-product from TPI isomerase activity, but its production is strongly increased by TPI nitrotyrosination [16]. Specifically, MG binds to and modifies arginine, cysteine, and lysine residues in proteins, which causes a non-enzymatic formation of different AGEs such as argpyrimidine, *Nε*- (carboxyethyl) lysine, hydroimidazolones *Nε*-(5-hydro-5-methyl-4-imidazolon-2-yl)-ornithine, and methyl-glyoxal-lysine dimer [30]. We studied the glycative modification of arginine to argpyrimidine as one of the most representative parameters of protein glycation due to MG. Here we analyzed the protein glycation in the cortex from an AD patient, confirming higher MG production than that of an age-matched, non-demented control (Fig. 1D); this concurs with previous results demonstrating protein glycation in AD brain [16]. Strong labeling for glycation was also observed in the hippocampus of an AD mouse model overexpressing (o.e.) AßPP and PS1 (Fig. 1E). Furthermore, high protein glycation was obtained when human neuroblastoma cells were challenged with Aβ oligomers (Fig 1F).

Aß treatment induces apoptosis in human neuroblastoma cells

Aβ aggregates are supposed to induce the characteristic neurodegeneration that produces AD [32]. Thus we addressed a study of the effects of Aβ oligomers on apoptosis in human neuroblastoma cells. First we studied cell viability after 24h challenges with increasing concentrations of Aβ oligomers (Fig. 2A). Aβ oligomers were significantly toxic for neuroblastoma cells from 0.1 to 1 μM and the toxicity was dose-dependent (Fig. 2A). These experiments were carried out in parallel with the study on glucose uptake (Fig.

S2), a parameter of the cell metabolism state. Glucose uptake was slight but significantly reduced with all the Aβ oligomers concentrations assayed in a pattern similar to that of cell viability.

Next we analyzed the reduction in cell viability induced by Aβ oligomers. One of the early intracellular events that occurs in apoptosis is the abnormal opening of the mitochondrial transition pore by the collapse of mitochondrial transmembrane potential ($\Delta\Psi m$), which results in a rapid release of caspase activators [32]. The pro-apoptotic effector Bax is a major mediator in this early apoptotic event. Bax levels were significantly increased when human neuroblastoma cells were challenged with Aβ oligomers (Fig. 2B). On the other hand, analysis of the protective anti-apoptotic protein Bcl-2 levels (Fig. 2B) showed that neuroblastoma cells had significantly decreased levels of Bcl-2 when challenged by Aβ oligomers, making them more prone to apoptosis.

Caspase-3 is down-stream of the activation of intracellular apoptotic pathways and has been shown to be elevated in AD model mice [33] and AD patient brains [34]. As expected after the proapoptotic changes we observed in mitochondria, Aβ oligomers significantly increased the levels of active caspase-3 compared to non-treated human neuroblastoma cells (Fig. 2C).

To confirm that TPI nitrotyrosination results from the Aβ-induced oxidative stress, we challenged neuroblastoma cells with scrambled $A\beta_{42}$, a scrambled peptide with the same aminoacids as in human $A\beta_{42}$, and cell viability was unchanged (Fig. S3A). As expected TPI nitrotyrosination was not increased by scrambled $A\beta_{42}$ treatment (Fig. S3B). Furthermore we challenged neuroblastoma cells with H_2O_2, an inducer of oxidative stress, and camptothecin, a proapoptotic inhibitor of DNA topoisomerase I. Both compounds triggered apoptosis (Fig. S4A and S4C) but only H_2O_2, which generates reactive oxygen species, induced TPI nitrotyrosination (Fig. S4D). To support the relevance of MG in Aß

toxicity, we preincubated neuroblastoma cells with aminoguanidine (AG) (Figs. 3 and S5), a well-known MG scavenger [35,36]. After 24h challenge with Aβ oligomers, we obtained a significant protection in cell viability when cells were preincubated with AG ($p<0.01$; Fig. 3A). Moreover, we analyzed the levels of pro- and anti-apoptotic proteins in the same conditions. Assayed by Western blot, preincubation with AG produced a significant increase in the protective Bcl-2 levels ($p<0.01$; Fig. 3B) and a decrease in the pro-apoptotics Bax and Caspase-3 ($p<0.05$ and $p<0.01$, respectively; Figs. 3B and 3C).

MG production is due to the nitration of the two tyrosines close to the catalytic center of the TPI

Aβ oligomers provoke the nitrotyrosination of TPI and this modified TPI produces an increase in the harmful by-product MG [16]. We studied how nitrotyrosination affects TPI to produce a burst of MG production. The TPI monomer has four tyrosines: Tyr47 and Tyr67 stay at the interface of the dimer in opposite orientations, so tyrosines from different monomers do not face each other, while the remaining Tyr165 and Tyr209 are interacting in a direct way and sit very close to the catalytic site, making them critical elements of catalytic dysfunction (Fig. S6).

To analyze the nitration ability of the two tyrosine residues in close proximity to the catalytic center, we used a proteomic-based mass spectrometry strategy. TPI protein was treated with SIN-1 (a peroxynitrite donor), then trypsinized and analyzed by LC-MS/MS (Fig. S7). Peptides assigned as being nitrated on tyrosine residues were validated manually: IIY(NO2)GGSVTGATCK (Fig. S7A) and VVLAY(NO2)EPVWAIGTGK (Fig. S7B). The LC-MS/MS experiment was not designed as a quantitative study. However, assuming no major difference in ionization and digestion efficiency of the tyrosine-nitrated

peptide compared to unmodified peptides, we used the area under the curve for each peptide to estimate the percentage of a residue that is modified. In our calculations, 5% to 8% of a given tyrosine residue was nitrated *in vitro*. This percentage is similar to the ~10% reported for nitrotyrosination in general *in vitro* assays [37].

On the other hand, computer models provide valuable understanding of protein activity, structure, and folding. They can also be used to study conformational changes induced by mutations or modifications of the protein and to predict if such alterations could have an effect on protein enzymatic activity. Having demonstrated that both tyrosines can be nitrated experimentally, we conducted a performed computational analysis of the conformational impact of nitrotyrosination on the catalytic domain of the enzyme. In addition, we confirmed that a double mutant TPI that we have generated, Y165F/Y209F mimics this new conformation and we validate it as a tool for understanding the impact of nitrotyrosination on cell viability. The tyrosines were substituted by phenylalanines because they have a similar size and structure, and Phe is not able to establish the biochemical interactions with the surrounded aminoacids, as nitro-Tyr does.

The TPI 3D structure defines the so-called "TIM barrel" fold, a regular eight-fold repeating pattern of ß-strands and α-helices. Loop 6 is very flexible and plays an important role in substrate binding and catalysis [38]. We hypothesized that TPI nitrotyrosination at Tyr165 and Tyr209 will destabilize the closed state of loop 6 [16], mainly due to the weakening of the H-bond interaction Tyr209-Ala177 (Fig. S6), and that this affects the efficiency of the enzyme. Furthermore, the electron withdrawal effect of the nitro substituent in the phenol ring of tyrosine must be a related factor. To test this hypothesis and to understand how the mutation of tyrosine by phenylalanine may be mimicking the effect of nitrotyrosination, we performed a battery of hybrid QM/MM structural calculations on the H-bond network around Tyr165 and Tyr209. Figure 4 summarizes the

results of the QM/MM calculations, which were conducted after short molecular dynamics (MD) simulations to relax the positions of the water molecules in the vicinity of the key hydrogen bonds (see Materials and methods). The figure is divided in two rows, corresponding to the closed state of TPI (upper row, Fig. 4A-C) and to its open state (lower row, Fig. 4D-F). The different subfigures show the relevant distances defining the hydrogen bond network after a standard MD protocol to relax the solvent molecules while keeping the substrate (the protein atoms) fixed, followed by minimization of a complete QM/MM system centered in the relevant H-bond.

The results for the closed state (based on simulations and minimization, PDB code 1NEY, see Experimental Procedures) show a reasonably similar environment around the Tyr209-Ala177 H-bond interaction in the different models (Fig. 4A-C). In fact, practically the same water molecules are found close to the H-bond. This helps to compare X209-Ala177 distances for the three systems with X=Tyr, Phe, NTyr. The distance between the hydroxyl oxygen in Tyr209 and the main chain N atom in Ala177 slightly increases when modified by nitrotyrosination of Tyr209, and the linearity of the H-Bond is also decreased (Fig. 4C). There are two reasons for this. On one hand, the electron withdrawal effect of the nitro group decreases the charge in the hydroxyl oxygen. On the other, the presence of competitor nitro oxygen essentially delocalizes this H-bond. Furthermore, the nitro group can exert a steric effect, which can perturb and destabilize the H-bond network. The increase in the X209-A177 distance is slightly larger for the Y209F substitution, as expected (Fig. 4B).

As for the open state, here the polarity of the environment around the Tyr165-Trp169 H-bond changes drastically in the mutated system Y165F and in the modified Y165*n* (with *n* representing nitrotyrosine) (Fig. 4D-F). For the wild-type system, the strongly polar environment produces a relatively mild H-bond interaction that keeps loop 6

in the open state (Fig. 4D). When we move to the Y165F mutant or to the nitrated tyrosine, the situation changes and the environment becomes relatively non-polar (Fig. 4E-F). This, in turn, enhances the interaction in the Y165*n*-W169 system, creating a stronger H-bond that may help to keep loop 6 in its open conformation for longer periods of time. In the case of the Y165F mutation, removing the Tyr165 hydroxyl group and reducing the polarity of the immediate environment helps the Phe165 residue to approach W169, compacting the system much the same as Y165*n* does.

Overall, Y209 and Y165 nitration helps to avoid the closure of loop 6 and to keep it open, respectively, producing the effect of increasing K_M (lower affinity of the ligand by its substrate) and decreasing k_{cat}/K_M (lower enzymatic activity) [16].

Increase in MG production in neuroblastoma cells transfected with the double mutant TPI

TPI nitrotyrosination results in reduced catalytic activity and increased occupancy of the enzyme by the substrate, and consequently, a higher production of toxic MG [16]. TPI prevents MG production by holding its loop 6 over the catalytic center when the substrate binds. Nitration of Tyr165 keeps loop 6 open via a hydrogen bond with Thr168, allowing the entry of water into the active site, which results in the hydrolysis of the intermediate enediol phosphate that yields MG.

This hypothesis was supported by the computational analysis and confirmed using human neuroblastoma cells o.e. WT and mutant TPI at Tyr165Phe and Tyr209Phe (YY TPI), the two nitrated residues close to the catalytic center (Fig. 5). These mutations mimic the effect of nitrotyrosination on loop stability.

Cells o.e. YY TPI showed an increase in MG production, detected by immunofluorescence (Fig. 5A) and Western blot (Fig. S8). MG diffuses easily. We found

that cells o.e. WT TPI incubated with conditioned medium from cells o.e. YY TPI showed wide protein glycation (Fig. 5A), but the same cells incubated with conditioned medium from cells o.e. WT TPI did not show any glycative stress (Fig. 5A). The effects of MG in cell death were also studied. We observed a reduction in cell viability when cells o.e. WT TPI were incubated with medium from cells o.e. YY TPI ($p<0.01$; Fig. 5B).

Increased apoptotic events in human neuroblastoma cells o.e. the double mutant TPI Y165F/Y209F

Considering that the double mutant Y165F/Y209F mimicked the MG production induced by Aβ-mediated TPI nitrotyrosination we analyzed the impact of mutant TPI expression on cell survival (Fig. 6). We observed a pattern consistent with a pro-apoptotic state: significant reduction in cell viability in cells transfected with the double mutant TPI compared to the WT TPI transfected cells (Fig. 6A). Moreover, we studied the apoptotic events, starting with the $\Delta\Psi_m$ (Fig. 6B). We found that cells o.e. double-mutant TPI had low $\Delta\Psi_m$ compared to cells o.e. WT TPI, suggesting a mitochondrial dysfunction. We also observed a significant increase in Bax levels and decrease in Bcl-2 in cells o.e. double-mutant TPI (Fig. 6C). These early apoptosis events were in accordance with the increase in active caspase-3 levels we observed in cells transfected with double-mutant TPI compared to WT-TPI transfected cells (Fig. 6D). A direct glycative effect on the studied apoptotic proteins (Bax, Bcl-2 and caspase-3) was discarded by Western blot analysis (Fig. S9).

No AD genetic risk associated with the TPI gene

Considering that TPI deficiencies have been associated with pathological neurologic symptoms [19,21] we analyzed the possible existence of TPI polymorphisms associated with AD (Table 1). As *TPI* is a small gene (~3 kilobases) located in a region with an estimated recombination rate of 3.0 cM/Mb, the genotyping of a single SNP would cover its genetic diversity. Our analysis did not disclose any significant differences in genotypes (χ^2=1.839, p=0.399) or allelic frequencies (χ^2=0.794, p=0.373) between cases and controls. These data support that TPI is a highly conserved protein due to its key role in glycolysis and any change is discarded rapidly due to its deleterious effects.

Discussion

Tyrosine nitration, an irreversible post-translational modification, is increased in AD [11,12] and the glycolytic TPI enzyme is one of the most nitrotyrosinated proteins in this disease [16,26,27]. TPI nitrotyrosination has a major consequence: it reduces glycolytic flow, which triggers production of MG, a compound associated with AD [16]. MG is produced by the formation of big protein aggregates due to cross-linking and by the decomposition of DHAP; its toxicity results from its ability to irreversibly modify proteins, lipids, and nucleic acids [39] (Fig. S10).

The TPI monomer has four tyrosines. The first two --Tyr47 and Tyr67-- remain at the interface of the dimer in opposite orientations, such that tyrosines from different monomers do not face each other, while the remaining two -- Tyr165 and Tyr209 -- interact directly, sit very close to the catalytic site, and contribute to loop 6 mobility. Loop 6 is very flexible and plays a key role in the reactivity of the enzyme [38]. We selected Tyr165 and Tyr209 for study because of their importance to enzyme efficiency and their role in MG generation. Our proteomic analysis showed that both tyrosines were nitrated when exposed to peroxynitrite.

In the present work, a combination of short classical MD simulations and QM/MM calculations helped us to predict the consequences of the nitrative modification in loop 6 of the TPI. We present a model showing how TPI nitrotyrosination at Tyr165 and Tyr209 would destabilize the closed state of the loop, affecting enzyme efficiency and promoting MG production. We also demonstrated that Tyr165Phe and Tyr209Phe mutations mimic the effect of nitrotyrosination on loop stability. Both situations were associated with increased production of the toxic compound, MG, which has the ability to irreversibly modify proteins, lipids, and nucleic acids.

When TPI efficiency is reduced, the substrate DHAP accumulates and is associated with increased MG production and, consequently, with protein glycation. It has been reported that MG rapidly glycates proteins, damages mitochondria, and induces a pro-oxidant state similar to that observed in aged cells [40]. This harmful scenario was present in the AD brain tissue [41] and high MG levels have been found in cerebrospinal fluid of patients affected by AD [42]. Glycation also has been associated with apoptosis [22,23], a pathologic process widely reported in AD [43]. Moreover, MG cytotoxicity has been associated with the impairment of cognitive function in diabetes [44].

We found TPI nitrotyrosination in AD patient cortex and in human neuroblastoma cells treated with Aβ oligomers. These findings were correlated with high protein glycation in AD patient cortex, in the hippocampus of double transgenic mice o.e. AßPP and PS1, and in human neuroblastoma cells treated with Aβ oligomers. These data suggest that TPI nitrotyrosination is playing a key role in the neurodegeneration triggered by Aβ. Cell viability declined consistently in human neuroblastoma cells transfected with the double-mutant TPI, which mimics the molecular effects of TPI nitrotyrosination. These results confirm existing evidence that apoptosis is the underlying mechanism for the neurodegeneration caused by TPI nitrotyrosination, reported in AD [43,45] and in Aβ-

induced nitro-oxidative stress [37,46]. Mitochondria play an essential role in cell death because the permeability of the transition pore and the collapse of $\Delta\Psi_m$ are the initial stages in intracellular apoptotic signalling [33]. Consistently we obtained a loss of $\Delta\Psi_m$ in TPI double-mutant cells, which was associated with an increase in Bax, a classical pro-apoptotic protein previously reported to be enhanced in AD [23]. We observed that Aβ oligomers and double-mutant TPI increased MG production by abnormal TPI function. Furthermore, we demonstrated that the increase of MG is related with the toxicity induced by Aß, resulting in increased levels of the active pro-apoptotic caspase-3. Caspase-3 is critical in apoptosis onset and a recent study links it to enhanced synaptic failure in an AD mouse model [47], which is a very early event in the disease onset. All these effects were reverted when cells were incubated with a MG scavenger, supporting evidence that MG is one of the most important intracellular mediators of Aβ-induced apoptosis. However, we cannot discard that other mechanisms are contributing to Aβ neurodegeneration.

On the other hand, once the MG burst is triggered there is a plethora of targets that could be glycated including proteins, lipids and nucleic acids [39]. One of the most relevant proteins for AD that can be glycated is tau, whose glycation has been proposed to favour its hyperphosphorylation and aggregation into neurofibrillary tangles [48-51]. All together will contribute to the characteristic neuronal damage of AD.

Finally, we analyzed the possibility that some polymorphisms in the TPI gene [52] could be associated with AD. Although its mutations correlate with neurological dysfunction, we observed no association between AD and the TPI gene, reinforcing the importance of post-translational modifications such as nitrotyrosination in the gene's observed relationship with AD onset and progression.

In conclusion, we have obtained the first results suggesting that Aβ oligomers induce neuronal death by triggering MG production. Increased release of MG is a direct

consequence of TPI nitrotyrosination due to Aβ action at the two tyrosines located in the catalytic center of the gene. MG leads to neuronal death by activating pro-apoptotic intracellular signalling. This finding links Aβ with neurodegeneration.

Acknowledgements

We thank Dr. Tadashi Nakaya and Dr. David Comas for their technical support. The authors acknowledge the computer resources, technical expertise and assistance provided by the Barcelona Supercomputing Center - Centro Nacional de Supercomputación. We also wish to acknowledge the Banc de Teixits Neurològics, Serveis Científico-Tècnics, Hospital Clínic, Universitat de Barcelona for providing the brain samples. This work was supported by the Spanish Ministry of Science and Innovation (SAF2010-16725; Fondo de Investigación Sanitaria PI10/00587 and PI10/01076; Red HERACLES RD12/0042/0014- FEDER Funds; CTQ2008-00755; BFU2006-28430-E/BMC and RETIC COMBIOMED RD07/0067/0001); the virtual physiological human (VPH) NoE (FP7-ICT-2007-2-223920); Generalitat de Catalunya (AGAUR BE-2 10240; SGR2009-1369); and La Marató de TV3 (Nº 100310 and 100610).

The authors declare that no competing financial interests exist.

References

[1] Huang X, Cuajungco MP, Atwood CS., Hartshorn MA, Tyndall JD, Hanson GR, Stokes KC, Leopold M, Multhaup G, Goldstein LE, Scarpa RC, Saunders AJ, Lim J, Moir RD, Glabe C, Bowden EF, Masters CL, Fairlie DP, Tanzi RE, Bush AI (1999) Cu(II) potentiation of alzheimer abeta neurotoxicity. Correlation with cell-free hydrogen peroxide production and metal reduction. *J Biol Chem* **274**, 37111-37116.

[2] Huang X, Atwood CS, Hartshorn MA, Multhaup G, Goldstein LE, Scarpa RC, Cuajungco MP, Gray DN, Lim J, Moir RD, Tanzi RE, Bush AI (1999) The A beta peptide of Alzheimer's disease directly produces hydrogen peroxide through metal ion reduction. *Biochemistry* **38**, 7609-7616.

[3] Varadarajan S, Yatin S, Kanski J, Jahanshahi F, Butterfield DA (1999) Methionine residue 35 is important in amyloid beta-peptide-associated free radical oxidative stress. *Brain Res Bull* **50**,133-141.

[4] Mattson MP (2004) Pathways towards and away from Alzheimer's disease. *Nature* **430**, 631-639.

[5] Yu JT, Chang RC, Tan L (2009) Calcium dysregulation in Alzheimer's disease: from mechanisms to therapeutic opportunities. *Prog Neurobiol* **89**, 240-255.

[6] Bredt DS, Snyder SH (1994) Nitric oxide: a physiologic messenger molecule. *Annu. Rev. Biochem* **63**, 175-195.

[7] Moncada S, Palmer RM, Higgs EA (1991) Nitric oxide: physiology, pathophysiology, and pharmacology 59. *Pharmacol Rev* **43**, 109-142.

[8] Beckman JS, Beckman TW, Chen J, Marshall PA, Freeman BA (1990) Apparent hydroxyl radical production by peroxynitrite: implications for endothelial injury from nitric oxide and superoxide. *Proc Natl Acad Sci USA* **87**, 1620-1624.

[9] Brennan ML, Wu W, Fu X, Shen Z, Song W, Frost H, Vadseth C, Narine L, Lenkiewicz E, Borchers MT, Lusis AJ, Lee JJ, Lee NA, bu-Soud HM, Ischiropoulos H, Hazen SL (2002) A tale of two controversies: defining both the role of peroxidases in nitrotyrosine formation in vivo using eosinophil peroxidase and myeloperoxidase-deficient mice, and the nature of peroxidase-generated reactive nitrogen species. *J Biol Chem* **277**, 17415-17427.

[10] Souza JM, Daikhin E, Yudkoff M, Raman CS, Ischiropoulos H (1999) Factors determining the selectivity of protein tyrosine nitration. *Arch Biochem Biophys* **371**, 169-178.

[11] Smith MA, Richey Harris PL, Sayre LM, Beckman JS, Perry G (1997) Widespread peroxynitrite-mediated damage in Alzheimer's disease. *J Neurosci* **17**, 2653-2657.

[12] Hensley K, Maidt ML, Yu Z, Sang H, Markesbery WR, Floyd RA (1998) Electrochemical analysis of protein nitrotyrosine and dityrosine in the Alzheimer brain indicates region-specific accumulation. *J Neurosci* **18**, 8126-8132.

[13] Quintanilla RA, Munoz FJ, Metcalfe MJ, Hitschfeld M, Olivares G, Godoy JA, Inestrosa NC (2005) Trolox and 17beta-estradiol protect against amyloid beta-peptide neurotoxicity by a mechanism that involves modulation of the Wnt signaling pathway. *J Biol Chem* **280**, 11615-11625.

[14] Huang TC, Lu KT, Wo YY, Wu YJ, Yang YL (2011) Resveratrol protects rats from Abeta-induced neurotoxicity by the reduction of iNOS expression and lipid peroxidation. *PLoS One* **6**, e29102.

[15] Coma M, Guix FX, Uribesalgo I, Espuna G, Sole M, Andreu D, Munoz FJ (2005) Lack of oestrogen protection in amyloid-mediated endothelial damage due to protein nitrotyrosination. *Brain* **128**, 1613-1621.

[16] Guix FX, Ill-Raga G, Bravo R, Nakaya T, de FG, Coma , Miscione GP, Villa-Freixa J, Suzuki T, Fernandez-Busquets X, Valverde MA, de SB, Munoz FJ (2009) Amyloid-dependent triosephosphate isomerase nitrotyrosination induces glycation and tau fibrillation. *Brain* **132**, 1335-1345.

[17] Richard JP (1993) Mechanism for the formation of methylglyoxal from triosephosphates. *Biochem Soc Trans* **21**, 549-553.

[18] Hoyer S (1996) Oxidative metabolism deficiencies in brains of patients with Alzheimer's disease. *Acta Neurol Scand Suppl* **165**, 18-24.

[19] Olah J, Orosz F, Puskas LG, Hackler L Jr, Horanyi M, Polgar L, Hollan S, Ovadi J (2005) Triosephosphate isomerase deficiency: consequences of an inherited mutation at mRNA, protein and metabolic levels. *Biochem J* **392**, 675-683.

[20] Seigle JL, Celotto AM, Palladino MJ (2008) Degradation of functional triose phosphate isomerase protein underlies sugarkill pathology. *Genetics* **179**, 855-862.

[21] Orosz F, Olah J, Ovadi J (2009) Triosephosphate isomerase deficiency: new insights into an enigmatic disease. *Biochim Biophys Acta* **1792,** 1168-1174.

[22] Kikuchi S, Shinpo K, Moriwaka F, Makita Z, Miyata T, Tashiro K (1999) Neurotoxicity of methylglyoxal and 3-deoxyglucosone on cultured cortical neurons: synergism between glycation and oxidative stress, possibly involved in neurodegenerative diseases. *J Neurosci Res* **57**, 280-289.

[23] Okouchi M, Okayama N, Aw TY (2005) Differential susceptibility of naive and differentiated PC-12 cells to methylglyoxal-induced apoptosis: influence of cellular redox. *Curr Neurovasc Res* **2**, 13-22.

[24] Yan SD, Yan SF, Chen X, Fu J, Chen M, Kuppusamy P, Smith MA, Perry G, Godman GC, Nawroth P, Zweier JL, Stern D (1995) Non-enzymatically glycated tau in Alzheimer's disease induces neuronal oxidant stress resulting in cytokine gene expression and release of amyloid beta-peptide. *Nat Med* **1**, 693-699.

[25] Stadtman ER (2001) Protein oxidation in aging and age-related diseases. *Ann NY Acad Sci* **928**, 22-38.

[26] Butterfield DA, Perluigi M, Sultana R (2006) Oxidative stress in Alzheimer's disease brain: new insights from redox proteomics. *Eur J Pharmacol* **545**, 39-50.

[27] Butterfield DA, Reed TT, Perluigi M, De MC, Coccia R, Keller JN, Markesbery WR, Sultana R (2007) Elevated levels of 3-nitrotyrosine in brain from subjects with amnestic mild cognitive impairment: implications for the role of nitration in the progression of Alzheimer's disease. *Brain Res* **1148**, 243-248.

[28] Rappsilber J, Mann M, Ishihama Y (2007) Protocol for micro-purification, enrichment, pre-fractionation and storage of peptides for proteomics using StageTips. *Nat Protoc* **2**, 1896-1906.

[29] Castegna A, Thongboonkerd V, Klein JB, Lynn B, Markesbery WR, Butterfield DA (2003) Proteomic identification of nitrated proteins in Alzheimer's disease brain. *J Neurochem* **85**, 1394-1401.

[30] Mukohda M, Okada M, Hara Y, Yamawaki H (2012) Exploring mechanisms of diabetes-related macrovascular complications: role of methylglyoxal, a metabolite of glucose on regulation of vascular contractility. *J Pharmacol Sci* **118**, 303-310.

[31] Fodero-Tavoletti MT, Villemagne VL, Rowe CC, Masters CL, Barnham KJ, Cappai R (2011) Amyloid-β: the seeds of darkness. *Int J Biochem Cell Biol* **43**, 1247-1251.

[32] Huang SM, Chuang HC, Wu CH, Yen GC (2008) Cytoprotective effects of phenolic acids on methylglyoxal-induced apoptosis in Neuro-2A cells. *Mol Nutr Food Res* **52**, 940-949.

[33] Bader Lange ML, St CD, Markesbery WR, Studzinski CM, Murphy MP, Butterfield DA (2010) Age-related loss of phospholipid asymmetry in APP(NLh)/APP(NLh) x PS-1(P264L)/PS-1(P264L) human double mutant knock-in mice: relevance to Alzheimer disease. *Neurobiol Dis* **38**, 104-115.

[34] Jarero-Basulto JJ, Luna-Muñoz J, Mena R, Kristofikova Z, Ripova D, Perry G, Binder LI, Garcia-Sierra F (2013) Proteolytic cleavage of polymeric tau protein by caspase-3: implications for Alzheimer disease. *J Neuropathol Exp Neurol* **72**, 1145-1161.

[35] Dhar A, Dhar I, Desai KM, Wu L (2010) Methylglyoxal scavengers attenuate endothelial dysfunction induced by methylglyoxal and high concentrations of glucose. *Br J Pharmacol* **161**, 1843-1856.

[36] de Arriba SG, Krugel U, Regenthal R, Vissiennon Z, Verdaguer E, Lewerenz A, Garcia-Jorda E, Pallas M, Camins A, Munch G, Nieber K, Allgaier C (2006) Carbonyl stress and NMDA receptor activation contribute to methylglyoxal neurotoxicity. *Free Radic Biol Med* **40**, 779-790.

[37] Alvarez B, Radi R (2003) Peroxynitrite reactivity with amino acids and proteins. *Amino Acids* **25**, 295-311.

[38] Alber T, Banner DW, Bloomer AC, Petsko GA, Phillips D, Rivers PS, Wilson IA (1981) On the three-dimensional structure and catalytic mechanism of triose phosphate isomerase. *Philos Trans R Soc Lond B Biol Sci* **293**, 159-171.

[39] Scheckhuber CQ, Mack SJ, Strobel I, Ricciardi F, Gispert S, Osiewacz HD (2010) Modulation of the glyoxalase system in the aging model Podospora anserina: effects on growth and lifespan. *Aging* **2**, 969-980.

[40] Hipkiss AR (2006) On the mechanisms of ageing suppression by dietary restriction-is persistent glycolysis the problem? *Mech Ageing Dev* **127**, 8-15.

[41] Caldeira GL, Ferreira IL, Rego AC (2013) Impaired transcription in Alzheimer's disease: key role in mitochondrial dysfunction and oxidative stress. *J Alzheimers Dis* **34**, 115-131.

[42] Rahmadi A, Steiner N, Münch G (2011) Advanced glycation endproducts as gerontotoxins and biomarkers for carbonyl-based degenerative processes in Alzheimer's disease. *Clin Chem Lab Med* **49**, 385-391.

[43] Su JH, Anderson AJ, Cummings BJ, Cotman CW (1994) Immunohistochemical evidence for apoptosis in Alzheimer's disease. *Neuroreport* **5**, 2529-2533.

[44] Chen YJ, Huang XB, Li ZX, Yin LL, Chen WQ, Li L (2010) Tenuigenin protects cultured hippocampal neurons against methylglyoxal-induced neurotoxicity. *Eur J Pharmacol* **645**, 1-8.

[45] LaFerla FM, Tinkle BT, Bieberich CJ, Haudenschild CC, Jay, G (1995) The Alzheimer's A beta peptide induces neurodegeneration and apoptotic cell death in transgenic mice. *Nat Genet* **9**, 21-30.

[46] Ill-Raga G, Ramos-Fernandez E, Guix FX, Tajes M, Bosch-Morato M, Palomer E, Godoy J, Belmar S, Cerpa W, Simpkins JW, Inestrosa NC, Munoz FJ (2010) Amyloid-beta peptide fibrils induce nitro-oxidative stress in neuronal cells. *J Alzheimers Dis* **22**, 641-652.

[47] D'Amelio M, Cavallucci V, Middei S, Marchetti C, Pacioni S, Ferri A, Diamantini A, De ZD, Carrara P, Battistini L, Moreno S, Bacci A, mmassari-Teule M, Marie H, Cecconi F (2011) Caspase-3 triggers early synaptic dysfunction in a mouse model of Alzheimer's disease. *Nat Neurosci* **14**, 69-76.

[48] Li XH, Lv BL, Xie JZ, Liu J, Zhou XW, Wang JZ (2012) AGEs induce Alzheimer-like tau pathology and memory deficit via RAGE-mediated GSK-3 activation. *Neurobiol Aging* **33**, 1400-1410.

[49] Kuhla B, Haase C, Flach K, Lüth HJ, Arendt T, Münch G (2007) Effect of pseudophosphorylation and cross-linking by lipid peroxidation and advanced glycation end product precursors on tau aggregation and filament formation. *J Biol Chem* **282**, 6984-6991.

[50] Ledesma MD, Medina M, Avila J (1996) The in vitro formation of recombinant tau polymers:effect of phosphorylation and glycation. *Mol Chem Neuropathol* **27**, 249-258.

[51] Ledesma MD, Bonay P, Avila J (1995) Tau protein from Alzheimer's disease patients is glycated at its tubulin-binding domain. *J Neurochem* **65**, 1658-1564.

[52] Orosz F, Olah J, Ovadi J (2006) Triosephosphate isomerase deficiency: facts and doubts. *IUBMB Life* **58**, 703-715.

Tables

Table 1

Genotype and allelic distribution of TPI SNP (rs2001004) analyzed in AD cases and control subjects

	AD Cases	Controls
Genotypes		
AA	105 (0.454)	54 (0.397)
AG	92 (0.398)	64 (0.471)
GG	34 (0.147)	18 (0.132)
Alleles		
A	302 (0.654)	172 (0.632)
G	160 (0.346)	100 (0.368)

Genotype and allele frequencies are expressed in brackets. Both groups were in Hardy-Weinberg equilibrium. Allele A showed an Odds Ratio of 1.097 (SE 0.159, Confidence Intervals 0.803-1.500) and a Relative Risk of 1.034 (SE 0.057, Confidence Intervals 0.924-1.137).

Figure Legends

Figure 1. TPI nitrotyrosination by Aβ and MG production. (A) Western blot of immunoprecipitated TPI from AD patient and non-demented (CT) frontal cortex. Quantifications are expressed as arbitrary units (AU). Data are mean ± SEM of 4 independent experiments. *** $p<0.001$ *vs* control by Student t test. (B) A representative image of intracellular TPI aggregates in AD frontal cortex analyzed by immunohistochemistry. (C) Western blot of immunoprecipitated TPI from SH-SY5Y cells treated with increasing concentrations of $A\beta_{42}$ oligomers for 24h. Blots were performed with anti-nitrotyrosine and anti-TPI Abs. Data are mean ± SEM of 3 independent experiments. * $p<0.05$, ** $p<0.01$ *vs* control by Student t test (D) AD patient and non-demented frontal cortex sections immunostained with an anti-argpyrimidine Ab. Positive staining is shown in AD patient (arrows). (E) Hippocampus from double transgenic mice o.e. AßPP and PS1 immunostained with an anti-argpyrimidine Ab. (F) Representative Western blot of SH-SY5Y cells challenged with 1 μM $A\beta_{42}$ oligomers for 24h. Glycation was analyzed using anti-argpyrimidine Ab.

Figure 2. Decreased cell viability and enhancement of apoptosis in neuroblastoma cells challenged with Aβ oligomers. (A) Cells challenged with increasing concentrations of Aβ oligomers assayed by MTT reduction. Data are mean ± SEM of 6 independent experiments performed in triplicate. ** $p<0.01$, *** $p<0.001$ *vs* control by Student t test. (B) Western blot analysis of pro-apoptotic Bax and anti-apoptotic Bcl-2 levels in cells challenged with increasing concentrations of Aβ oligomers. Quantifications expressed as AU are shown in the graphs. Data are mean ± SEM of 6 independent experiments.* $p<0.05$, ** $p<0.01$, *** $p<0.001$ *vs* control by Student t test. (C) Western blot analysis

of activated caspase-3 levels in cells treated with Aβ (A) at different concentrations. It was quantified and expressed as AU. Data are mean ± SEM of 6 independent experiments.* $p<0.05$, ** $p<0.01$, *** $p<0.001$ by Student t test.

Figure 3. Decreased Aβ toxicity on neuroblastoma cells pretreated with AG, a MG scavenger. (A) Cell viability assay by MTT reduction after 24 hr of Aβ treatment. Data are mean ± SEM of 6 independent experiments performed in triplicate. * $p<0.001$ *vs* control; ## $p<0.01$ *vs* Aβ treated cells by Student t test. (B) Western blot analysis of Bax and Bcl-2 levels in cells challenged with Aβ oligomers and Aβ plus AG for 24 hr. Quantifications expressed as AU are shown in the graphs. Data are mean ± SEM of 6 independent experiments.* $p<0.001$ *vs* control; # $p<0.05$, ## $p<0.01$ *vs* Aβ treated cells by Student t test. (C) Western blot analysis of activated caspase-3 levels in cells treated with Aβ and Aβ plus AG. It was quantified and expressed as AU. Data are mean ± SEM of 6 independent experiments.* $p<0.001$ vs control; ## $p<0.01$ *vs* Aβ treated cells by Student t test.

Figure 4. Computational modelling of the effect of Phe and nitroTyr substitutions on Tyr165 and Tyr209. Equilibrium structures obtained by hybrid QM/MM optimizations of the regions surrounding the two key hydrogen bonds in which Tyr165 and Tyr209 are, respectively, involved. The first row corresponds to the region containing the characteristic Y209-A177 HB in the closed state (based on the structure with PDB code 1NEY) in three different systems, namely (A) wt TPI, (B) Y209F and (C) Y209*n*, with *n* = nitrotyrosine. The second row corresponds to the region containing the characteristic Y165-W169 HB in the open state (based on the structure with PDB code

1I45) in three different systems, namely (D) wt TPI, (E) Y165F, and (F) Y165n. Images were produced with Chimera.

Figure 5. MG production in neuroblastoma cells o.e. WT or YY TPI. (A) Cells were untreated, treated with AG, or incubated with conditioned media from cells o.e. WT TPI or YY TPI. Glycation was studied with an anti-argpyrimidine Ab (red staining). pcDNA3 was used as the transfection control. Transfected cells were EGFP positive (green staining). Images were analyzed by confocal microscopy. (B) Cell viability of normal transfected cells or incubated with the conditioned medium from cells o.e. YY TPI. It was assayed by MTT reduction. Data are mean ± SEM of 3 independent experiments performed in triplicate. * $p<0.01$ *vs* control; # $p<0.01$ *vs* WT TPI by Student t test.

Figure 6. Increased apoptosis in neuroblastoma cells o.e. double-mutant TPI Y165F/Y209F. (A) Cell viability measurement of the transfected cells. Data are mean ± SEM of 3 independent experiments performed in triplicate. * $p<0.01$ *vs* cells o.e. WT TPI by Student t test. (B) Representative graph of $\Delta\Psi m$ in cells o.e. WT TPI or YY TPI assayed by flow cytometry and MitoTracker staining. The quantification of cells with low $\Delta\Psi m$ is expressed as percentage of WT TPI. Data are mean ± SEM of 4 independent experiments performed in triplicate. * $p< 0.05$ *vs* cells o.e. WT TPI by Student t test. (C, D) Western blot analysis of Bax, Bcl-2 (C) and caspase-3 (D) levels in cells o.e. WT TPI or YY TPI. Quantifications expressed as arbitrary units (AU) are shown in the graphs. Data are mean ± SEM of 4 independent experiments. * $p<0.05$; ** $p<0.01$; *** $p<0.001$ *vs* cells o.e. WT TPI by Student t test.

Supplementary Data

Figure S1. $A\beta_{42}$ oligomer characterization. Western blot of $A\beta_{42}$ oligomers. Anti-Aß Ab was used to validate the species selected for cell treatment. Oligomer bands are shown.

Figure S2. Glucose uptake in neuroblastoma cells. Glucose uptake in cells treated with increasing concentrations of Aß oligomers. Glucose uptake was quantified and expressed as (AU). Data are mean ± SEM of 4 independent experiments. * $p< 0.05$, ** $p< 0.01$ *vs* control by Student t test.

Figure S3. The scrambled $A\beta_{42}$ cannot induce the nitrotyrosination of TPI. (A) Neuroblastoma cells were challenged with increasing concentrations of scrambled $A\beta_{42}$ for 24h. Cell viability was assayed by MTT reduction. Data are mean ± SEM of 3 independent experiments performed in triplicate. (B) Western blot of immunoprecipitated TPI from neuroblastoma cells treated with increasing concentrations of scrambled $A\beta_{42}$ for 24h. Blots were performed with anti-nitrotyrosine and anti-TPI Abs. Data are mean ± SEM of 3 independent experiments

Figure S4. Nitrotyrosination of TPI is due to nitro-oxidative stress. (A) Neuroblastoma cells were challenged with increasing concentrations of camptothecin, a proapoptotic compound, and H_2O_2, a pro-oxidant compound, for 24h. Cell viability was assayed by MTT reduction. Data are mean ± SEM of 3 independent experiments performed in

triplicate. * $p<0.05$, ** $p<0.001$ by Student t test. (B) Western blot of immunoprecipitated TPI from neuroblastoma cells treated with increasing concentrations of camptothecin and H_2O_2 for 24h. Blots were performed with anti-nitrotyrosine and anti-TPI Abs.

Figure S5. Aminoguanidine dose-response curve. Neuroblastoma cells were treated with increasing concentrations of AG. Cell viability was assayed by MTT reduction. Data are mean ± SEM of 3 independent experiments performed in triplicate. * $p<0.01$, ** $p<0.001$ *vs* control by Student t test.

Figure S6. Loop 6 conformational changes in TPI. Image of the loop in the open/closed state showing the distances between the amidic nitrogen NH of Ala176 and the Oη oxygen of Tyr209 in both states.

Figure S7. Proteomic analysis of TPI nitrotyrosination. TPI was treated *in vitro* with SIN-1 as indicated in the Material and Methods section. Annotated tandem MS (HCD) spectra of two tryptic tyrosine nitrosylated peptides originating from TPI are shown: (A) IIY(NO2)GGSVTGATCK and (B) VVLAY(NO2)EPVWAIGTGK. In the spectra, vertical lines indicate y-ions used for the manual validation of the peptide sequences. Deduced peptide sequences (from C-terminal to N-terminal) are inserted above each spectrum. $Y(NO_2)$ indicate a nitrosylated tyrosine residue. Additional a- and b-ions are marked.

Figure S8. Increased protein glycation in cells o.e. YY TPI. Cells o.e. the double mutant TPI Y165F/Y209F were lysed and the total protein was analyzed by Western

blot using an anti-argpyrimidine Ab. Glycation was quantified and expressed as (AU). Data are mean ± SEM of 3 independent experiments. *$p<0.05$ vs controls by Student t test.

Figure S9. Lack of glycation in apoptotic proteins from cells o.e. double-mutant TPI Y165F/Y209F. Western blot analysis of Bax (A), Bcl-2 (B) and caspase-3 (C) levels in cells o.e. pcDNA3, WT TPI or YY TPI. Blots were performed with anti-argpyrimidine and anti-Bax (A), anti-Bcl-2 (B) or anti-caspase-3 (C) Abs. Quantifications expressed as arbitrary units (AU) are shown in the graphs. Data are mean ± SEM of 3 independent experiments.

Figure S10. TPI activity in physiological and pathological states. (A) Under physiological conditions MG production by the non-enzymatic decomposition of DHAP is very low, and the correct function of TPI allows the continuity of the glycolysis pathway. (B) Under pathological conditions, Aβ induces TPI nitrotyrosination. This posttranslational modification diminishes its efficiency and increases the production of the toxic by-product MG, which leads to neuronal apoptosis.

Figure 1

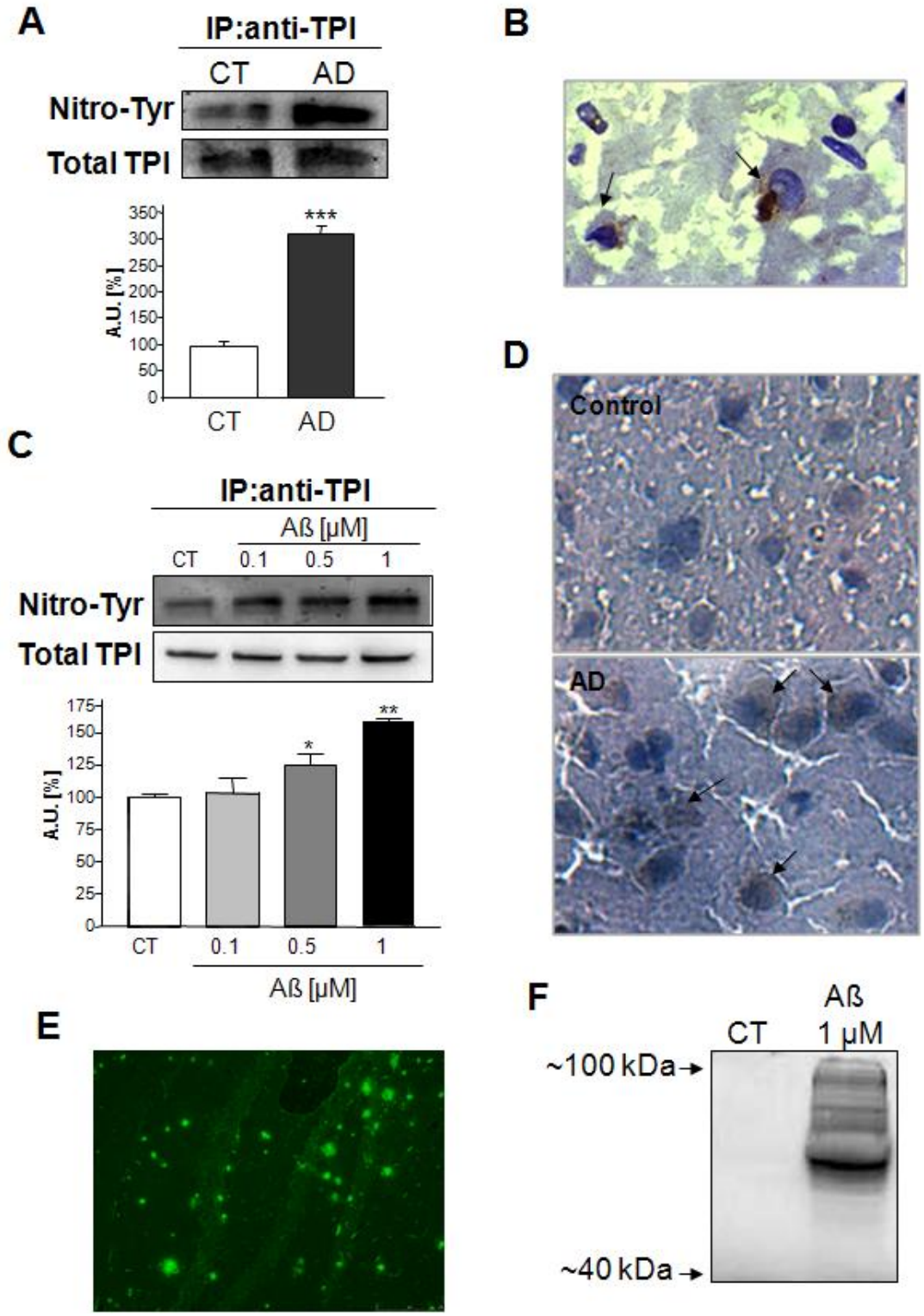
A
IP:anti-TPI
CT
AD
Nitro-Tyr
Total TPI
A.U. [%]
***
B
C
IP:anti-TPI
Aß [µM]
CT
0.1
0.5
1
Nitro-Tyr
Total TPI
A.U. [%]
*
**
D
Control
AD
E
F
Aß
1 µM
~100 kDa
~40 kDa

Figure 2

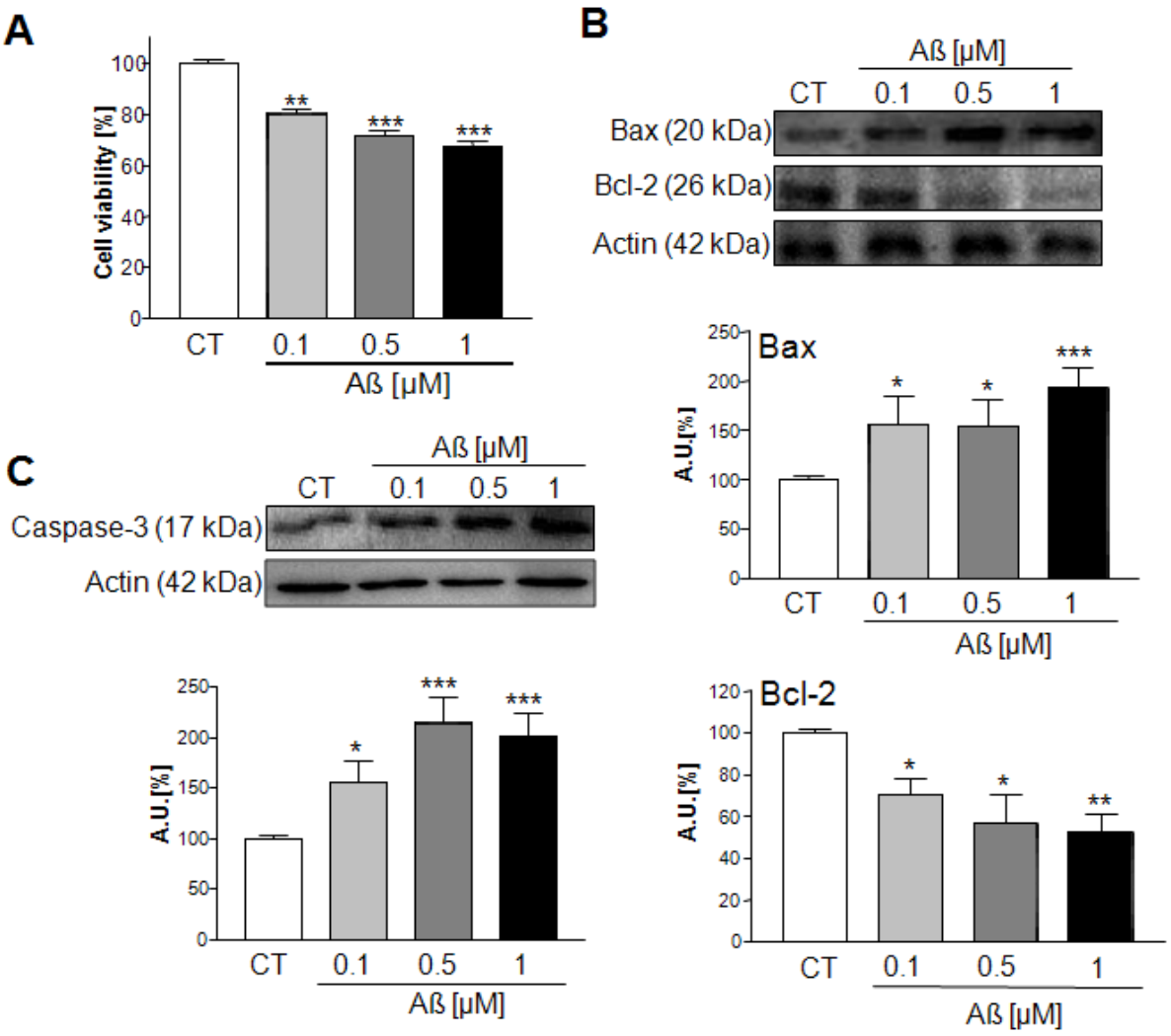
A
Cell viability [%]
100
80
60
40
20
0
**
***
***
CT
0.1
0.5
1
Aß [µM]
B
Aß [µM]
CT
0.1
0.5
1
Bax (20 kDa)
Bcl-2 (26 kDa)
Actin (42 kDa)
Bax
A.U.[%]
250
200
150
100
50
0
*
*
***
CT
0.1
0.5
1
Aß [µM]
C
Aß [µM]
CT
0.1
0.5
1
Caspase-3 (17 kDa)
Actin (42 kDa)
A.U.[%]
250
200
150
100
50
0
*
***
***
CT
0.1
0.5
1
Aß [µM]
Bcl-2
A.U.[%]
120
100
80
60
40
20
0
*
*
**
CT
0.1
0.5
1
Aß [µM]

Figure 3

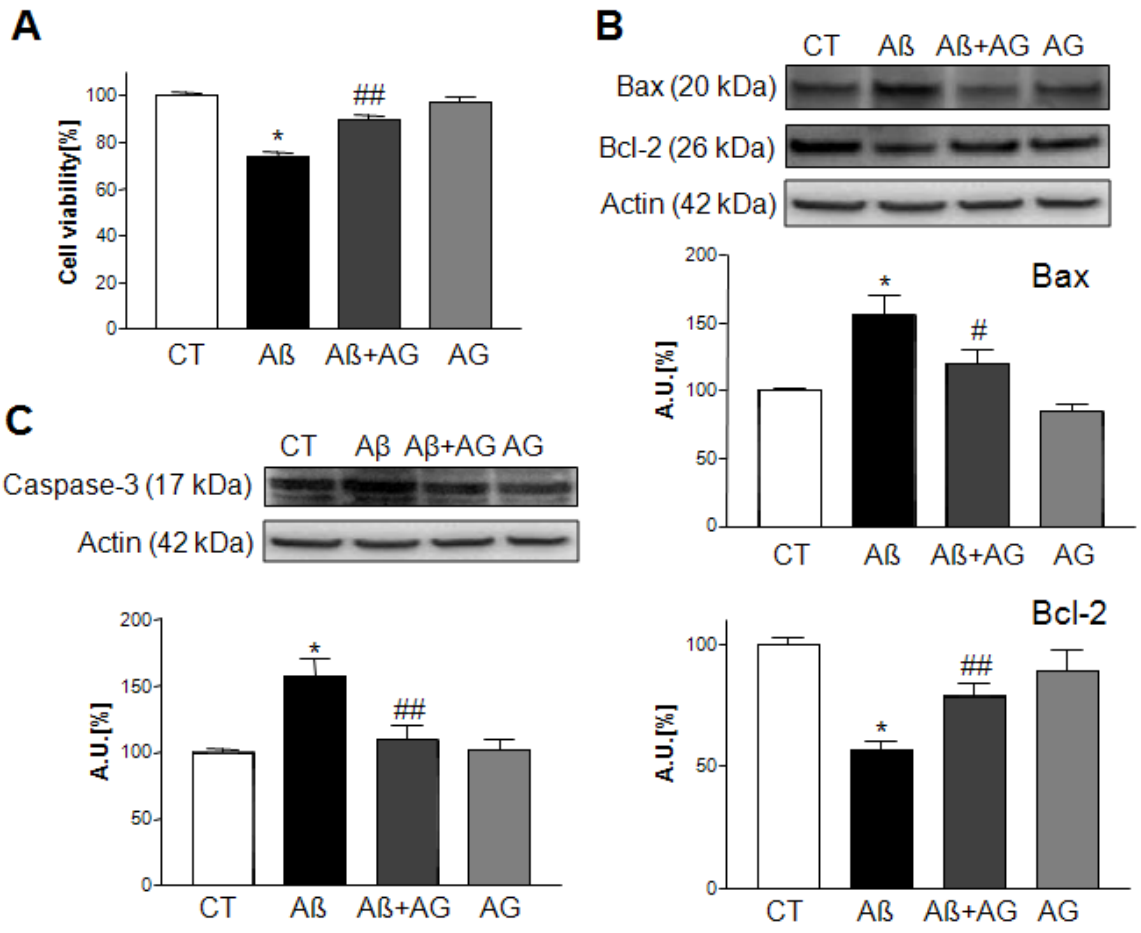
A
Cell viability[%]
100
80
60
40
20
0
*
##
CT
Aß
Aß+AG
AG
B
CT
Aß
Aß+AG
AG
Bax (20 kDa)
Bcl-2 (26 kDa)
Actin (42 kDa)
Bax
A.U.[%]
200
150
100
50
0
*
#
CT
Aß
Aß+AG
AG
C
CT
Aß
Aß+AG
AG
Caspase-3 (17 kDa)
Actin (42 kDa)
A.U.[%]
200
150
100
50
0
*
##
CT
Aß
Aß+AG
AG
Bcl-2
A.U.[%]
100
50
0
*
##
CT
Aß
Aß+AG
AG

Figure 4

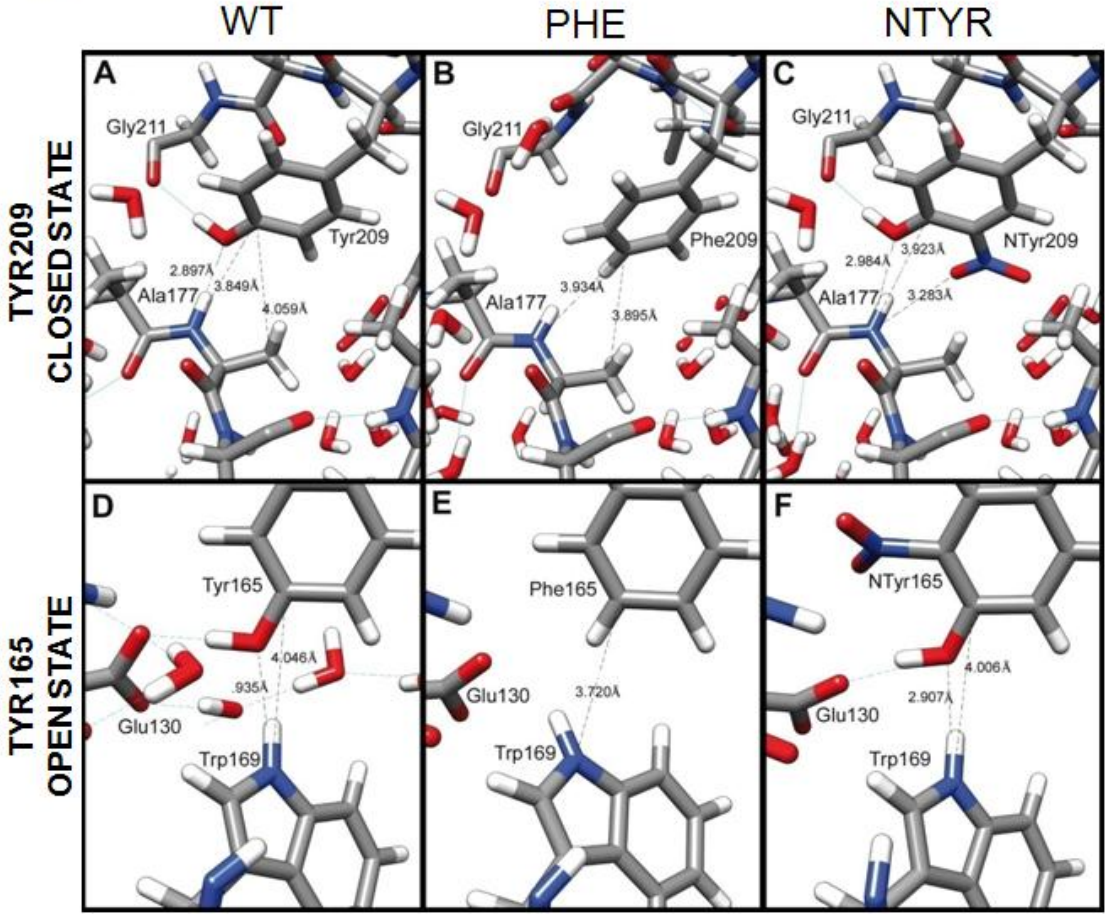
WT
PHE
NTYR
TYR209 CLOSED STATE
TYR165 OPEN STATE
A
B
C
D
E
F
Gly211
Tyr209
Phe209
NTyr209
Ala177
Tyr165
Phe165
NTyr165
Glu130
Trp169
2.897Å
3.849Å
4.059Å
3.934Å
3.895Å
2.984Å
3.923Å
3.283Å
4.046Å
.935Å
3.720Å
4.006Å
2.907Å

Figure 5

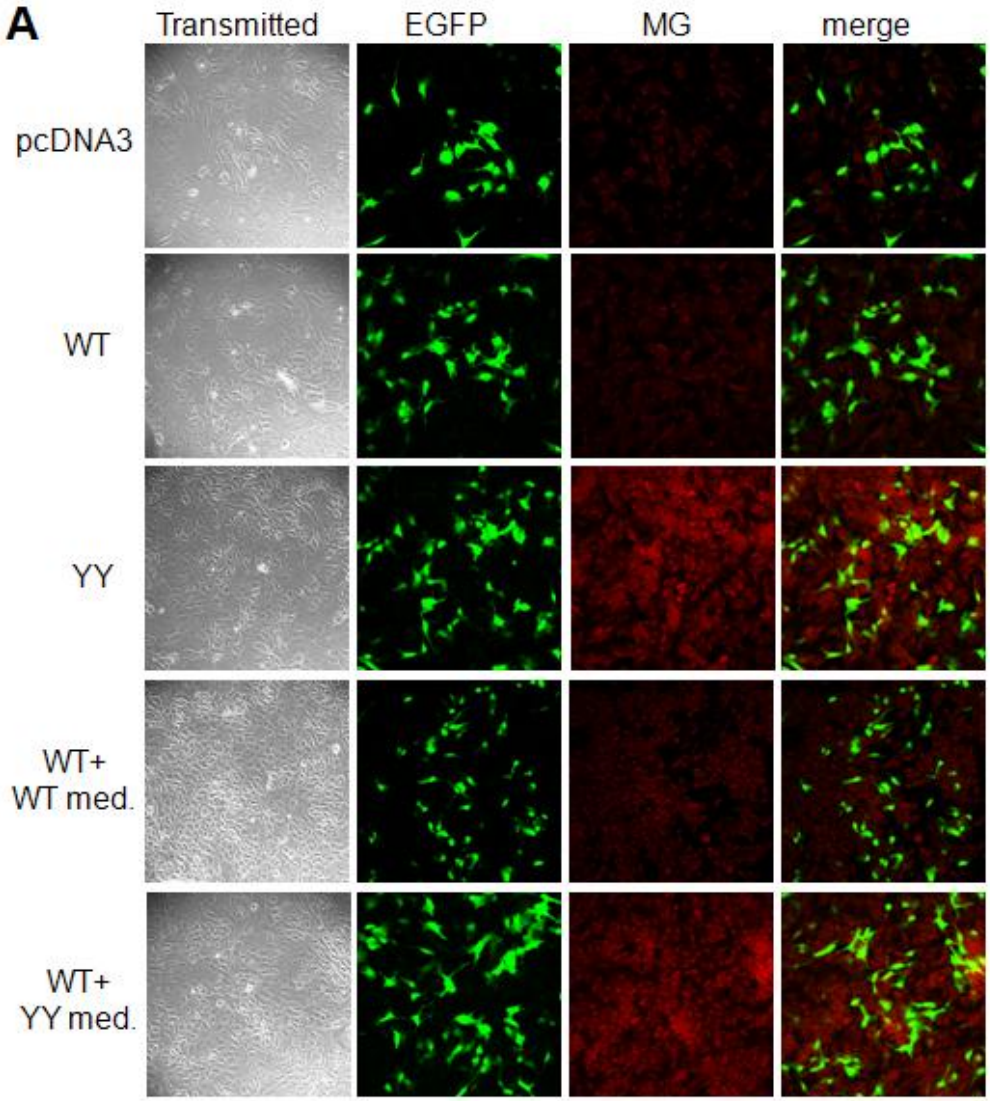
A
Transmitted
EGFP
MG
merge
pcDNA3
WT
YY
WT+
WT med.
WT+
YY med.

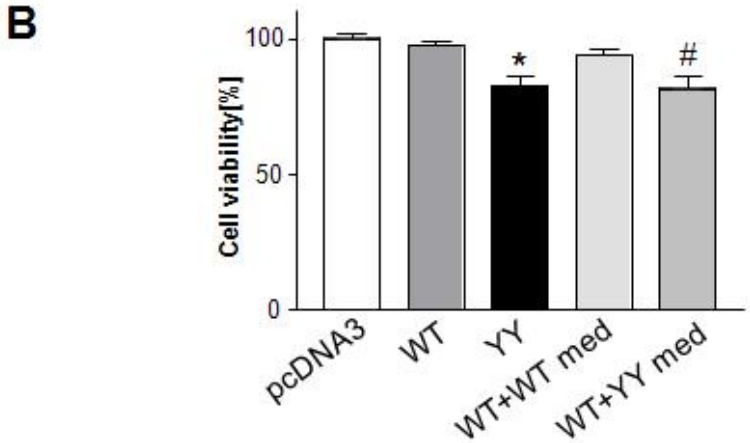
B
Cell viability[%]
100
50
0
*
#
pcDNA3
WT
YY
WT+WT med
WT+YY med

Figure 6

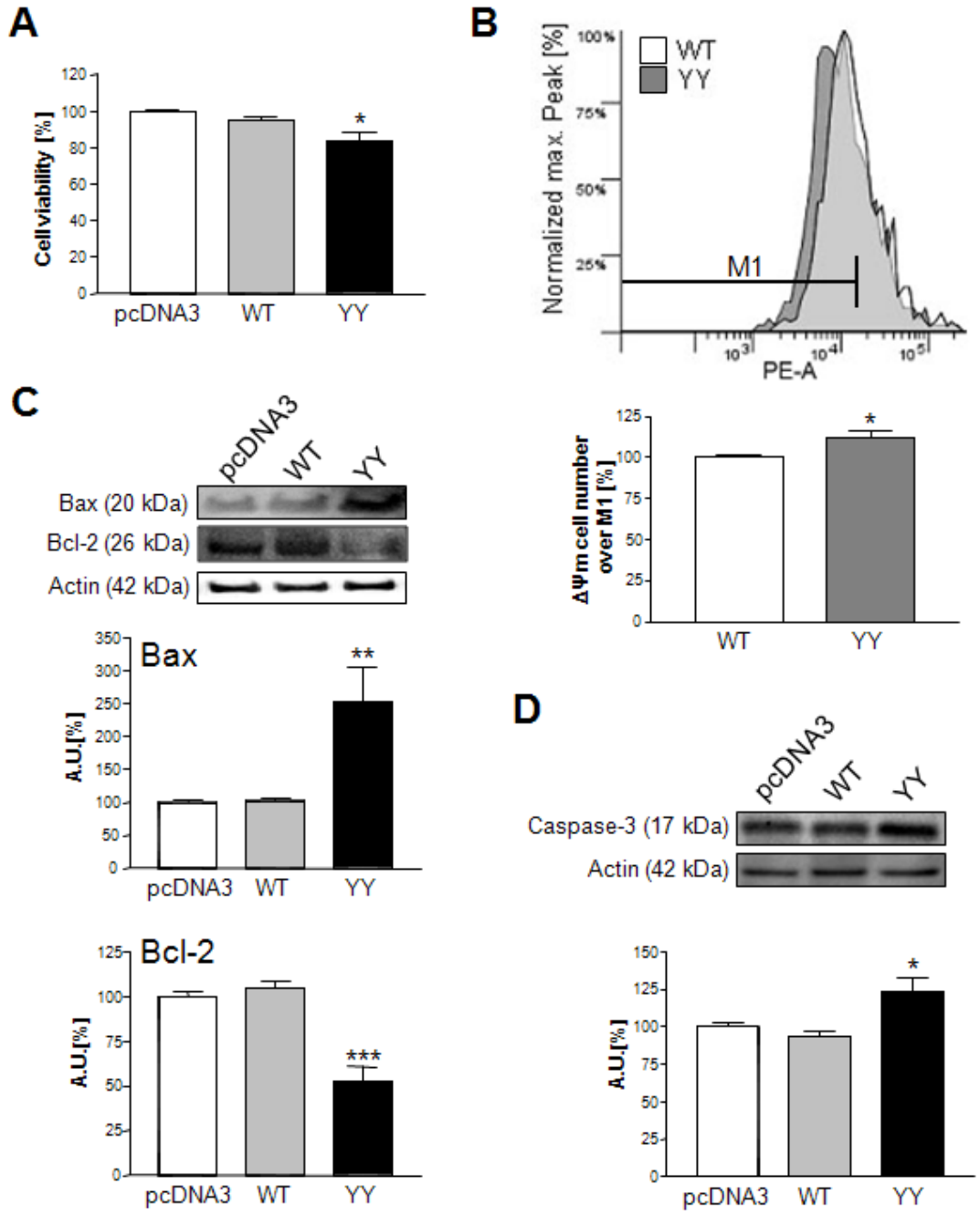
A
Cell viability [%]
120
100
80
60
40
20
0
*
pcDNA3
WT
YY
B
Normalized max. Peak [%]
100%
75%
50%
25%
WT
YY
M1
10^3
10^4
10^5
PE-A
ΔΨm cell number over M1 [%]
125
100
75
50
25
0
*
WT
YY
C
pcDNA3
WT
YY
Bax (20 kDa)
Bcl-2 (26 kDa)
Actin (42 kDa)
Bax
A.U.[%]
350
300
250
200
150
100
50
0
**
pcDNA3
WT
YY
Bcl-2
A.U.[%]
125
100
75
50
25
0
***
pcDNA3
WT
YY
D
pcDNA3
WT
YY
Caspase-3 (17 kDa)
Actin (42 kDa)
A.U.[%]
150
125
100
75
50
25
0
*
pcDNA3
WT
YY